High-Speed W-Band Integrated Photonic Transmitter for Radio-Over-Fiber Applications

Nan-Wei Chen, *Member, IEEE*, Hsuan-Ju Tsai, Fon-Ming Kuo, and Jin-Wei Shi, *Member, IEEE*

***Abstract*—A high-speed W-band integrated photonic transmitter is demonstrated. The presented integrated photonic transmitter is essentially developed with a near-ballistic uni-traveling-carrier photodiode integrated with a broadband front end through the flip-chip assembling technique. Technically, compared to our previous design, a W-band bandpass filter is exploited to significantly increase the transmitter IF modulation bandwidth. The demonstrated integrated photonic transmitter has a flat broad IF modulation response, as well as a broad optical-to-electrical (O-E) bandwidth. Specifically, the variation of the normalized IF modulation response, ranging from dc to around 13 GHz, is within 3 dB, and the normalized 3-dB O-E bandwidth is about 24 GHz. On the other hand, an up to 20-Gb/s high data-rate wireless transmission realized with the presented transmitter is demonstrated. The integrated photonic transmitter is expected to find applications in high-speed radio-over-fiber communications.**

***Index Terms*—Front-end, photonic transmitter, radio-over-fiber (RoF), uni-traveling-carrier photodiode (UTC-PD), W-band.**

I. Introduction

RADIO-OVER-FIBER (RoF) communication systems [1]–[9] are considered as one of the most suitable candidates for the next generation of gigabit wireless access. The RoF system calls for a high-speed integrated photonic transmitter of wide optical-to-electrical (O-E) and IF modulation bandwidth for the development of a high data-rate wireless transmission at the last mile. In this regard, the photodiodes (PDs) of high speed and high saturation current [10]–[14] integrated with high-gain transmitting antennas [15]–[18] and passive circuits have been employed for realization of the transmitters of this sort. These transmitters essentially are comprised of the uni-traveling-carrier photodiodes (UTC-PDs) integrated with a classical high-gain antenna such as the lens-integrated slot antenna [18], [19] and the planar quasi-Yagi antenna [20]–[22]. It is shown that the implementation of a photonic transmitter with wide O-E and IF modulation/video bandwidth requires accurate system characterization that simultaneously includes both high-frequency (optical) and relatively low-frequency (electrical) analyses. Specifically, the accurate PD optical modeling, especially regarding the transients as well as parasitics attributed to its metallic structures and flip-chip bond pads, and the full-wave electrical characterization of the front end, including the transmitting antenna and passive circuits, are crucial to a successful design. As for the front-end design, the good isolation between the IF signal input and local oscillator (LO) source output appears to be the key to the realization of a wide video bandwidth of the transmitter.

In this paper, a W-band integrated photonic transmitter with wide O-E and IF bandwidths for an up to 20-Gb/s high data-rate transmission is presented. The demonstrated transmitter comprises broadband front-end circuitry and the traditional waveguide-based horn antenna fed by a dipole-based structure for the realization of the directional radiation from the integrated photonic transmitter. The antenna feed structure is planar in nature and poised for easy integration with a near-ballistic uni-traveling carrier photodiode (NBUTC-PD) [11], [12] via a flip-chip bonding technique. Indeed, compared to the related past works [23]–[26], the proposed waveguide feed does not require any modifications to the waveguide connected to the horn antenna, as well as bond wires on the feed structure, which appears to be critical to a relatively easy and low-cost front-end implementation. As for front-end circuitry, compared to our previous works, a W-band bandpass filter (BPF) is employed for improving the isolation between the IF signal input and LO source input, which results in a significant improvement on the video bandwidth. For system design, each passive circuit block of the front end is designed with the equivalent transmission-line circuit representation and realized with the slotline structure. Regarding system characterization, the S-parameter data of each developed circuit block is accurately extracted with the full-wave analysis. The entire system is then represented by a network comprised of the developed blocks with their extracted S-parameter data in a cascaded topology, and hence, the circuit solver can be used to characterize the transmitter in a relatively effective manner. At the final design stage, the full-wave system characterization is employed for verification of the results from the circuit simulation.

This paper is organized as follows. Section II details the proposed W-band integrated photonic transmitter design. Section III describes the experimental setup for system characterization and presents the measurement results. Finally, Section IV draws the conclusions of this work and outlines future works.

Manuscript received October 31, 2010; accepted December 02, 2010. Date of publication February 04, 2011; date of current version April 08, 2011. This work was supported in part by the National Science Council of Taiwan under Contract NSC98-2221-E-155-075-MY3, Contract NSC98-2221-E-008-009-MY3, Contract NSC99-2120-M-002-013, and Contract NSC98-2221-E-007-025-MY3. This paper is an expanded paper from the IEEE MTT-S International Microwave Symposium, Anaheim, CA, May 23–28, 2010.

N.-W. Chen is with the Department of Communications Engineering, Yuan Ze University, Jhongli 32003, Taiwan (e-mail: nwchen@saturn.yzu.edu.tw).

H.-J. Tsai, F.-M. Kuo, and J.-W. Shi are with the Department of Electrical Engineering, National Central University, Jhongli 32004, Taiwan (e-mail: shamyah@hotmail.com; 975201125@cc.ncu.edu.tw; jwshi@ee.ncu.edu.tw).

Color versions of one or more of the figures in this paper are available online at http://ieeexplore.ieee.org.

Digital Object Identifier 10.1109/TMTT.2011.2104977

II. System Design and Analysis

Fig. 1(a) depicts the 3-D schematic diagram of the diced NBUTC-PD module, as well as the front-end circuitry of the demonstrated W-band integrated photonic transmitter. The NBUTC-PD module includes the NBUTC-PD integrated with a microlens on an indium phosphide (InP) substrate. The module is integrated with the front end through the flip-chip bond pillars and slotline bond pads. The corresponding schematic system building-block diagram is shown in Fig. 1(b). In Fig. 1(b), the NBUTC-PD is illuminated by an optical millimeter-wave (MMW) W-band source focused with a microlens and delivered through a single-mode optical fiber. Meanwhile, the IF signal passing through a W-band bandstop filter (BSF), also termed as the RF choke, is pumped into the NBUTC-PD for the optical MMW source modulation. Here, the NBUTC-PD essentially functions like an opto-electronic mixer of the transmitter [16], [28]. The modulated W-band source passing through a W-band BPF is then forwarded to the waveguide feed of the horn antenna. Again, the BPF employed herein is for isolation enhancement between the IF port and waveguide feed structure. In our previous work [16], [21], the partially reflected W-band source from the feed is filtered out by the RF choke regarding the input signal integrity. However, the IF signal is not completely delivered to the PD for bias modulation since a fractional amount of the power leaks to the waveguide feed. With the BPF, the IF power leakage is alleviated. In other words, the isolation between the IF port and the waveguide feed is further enhanced, which leads to a significant improvement on the video bandwidth of the transmitter.

In what follows, the design and analysis of the proposed W-band integrated photonic transmitter are detailed. Specifically, the NBUTC-PD modeling and the design along with characterization of each front-end circuit block are, respectively, presented in Sections II-A and B. Finally, Section II-C describes the system characterization.

A. NBUTC-PD

Again, the NBUTC-PD, viz. the opto-electronic mixer of the transmitter, is employed for efficient optical to MMW power conversion. The NBUTC-PD with a large saturation current-bandwidth product can be realized with a thin depletion layer and the reduction of the device active area [12]. The thin depletion layer features a shorter carrier transit time and a higher saturation current performance, while the small active area reduces the junction capacitance for high-speed applications. In Fig. 1(a), the 900 μm $\times$ 900 μm diced NBUTC-PD module includes a 12 μm $\times$ 12 μm PD active region and the integrated microlens of a radius 135 μm. The PD responsivity and 3-dB bandwidth are 0.15 A/W and 110 GHz, respectively. The detailed configuration and dimensions of the NBUTC-PD are provided in [12], where many parameter choices of the PD design are also elucidated and justified. As mentioned above, the design of the photonic transmitter, i.e., the NBUTC-PD integrated with the front end, calls for both optical and electrical characterization. In [11], an equivalent three-port lumped-circuit model was proposed for the representation of the NBUTC-PD connected with coplanar-waveguide (CPW) bond pads. The optical characteristics of the NBUTC-PD, such as the limited bandwidth

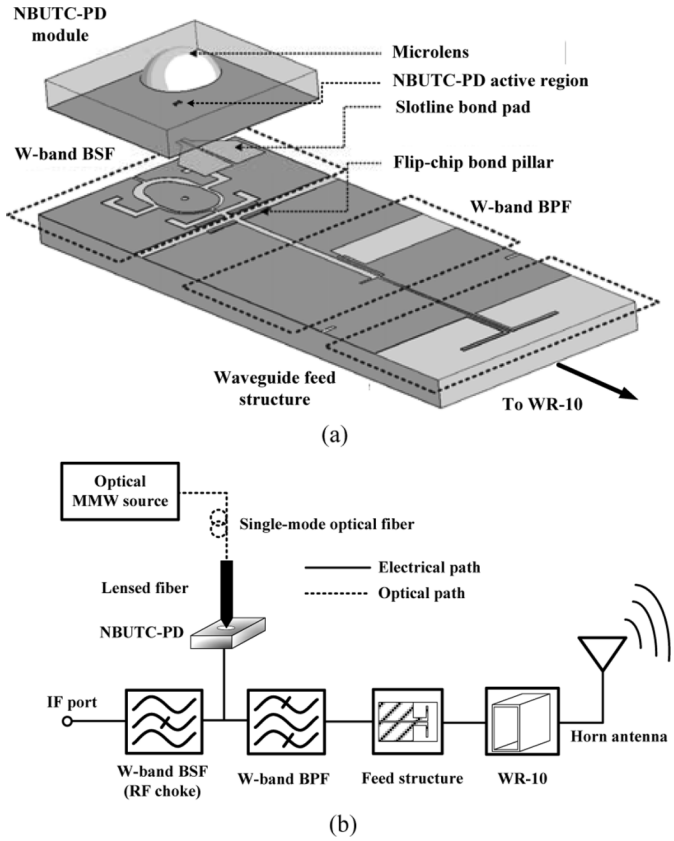

Fig. 1. (a) 3-D schematic diagram of the proposed W-band integrated photonic transmitter comprised of the NBUTC-PD and the front-end circuitry. (b) Corresponding schematic system building-block diagram.

owing to its carrier transit time and *RC* delay time, is modeled by an *RC* network, while the lumped-circuit representation of the electrical characteristics of the NBUTC-PD over the whole system operating bandwidth (W-band) is obtained by curve fitting the measured input impedance of the NBUTC-PD with the CPW bond pads. However, this design requires a CPW to slotline transition for the connection between the PD module and waveguide feed structure. It is shown that the broadband aperture-like transition leads to a high insertion loss owing to its relatively strong radiation at the MMW frequency regime. Here, the slotline structure is adopted to avoid the use of the transition.

Below, a modified electrical modeling of NBUTC-PD module [see Fig. 2(a)] with the slotline bond pads is described. On the contrary to the above-mentioned model development, viz. the solely lumped-circuit modeling, the PD module is firstly represented by a two-port network [see Fig. 2(b)] along with lumped-circuit elements. With this two-port network, as depicted in Fig. 1(b), the entire transmitter is then represented as a three-port network since one of the ports is for the IF signal input, as well as the LO source output. The detailed development of the PD network development is presented as follows. Fig. 2(a) depicts the PD structure without the integrated microlens. A ground–signal (G-S) wafer probe is used to extract the input impedance of the unilluminated PD structure on a supporting metallic plate. The slotline bond pads are on a 2.5-μm-thick benzocyclobutene (BCB) film. The active region

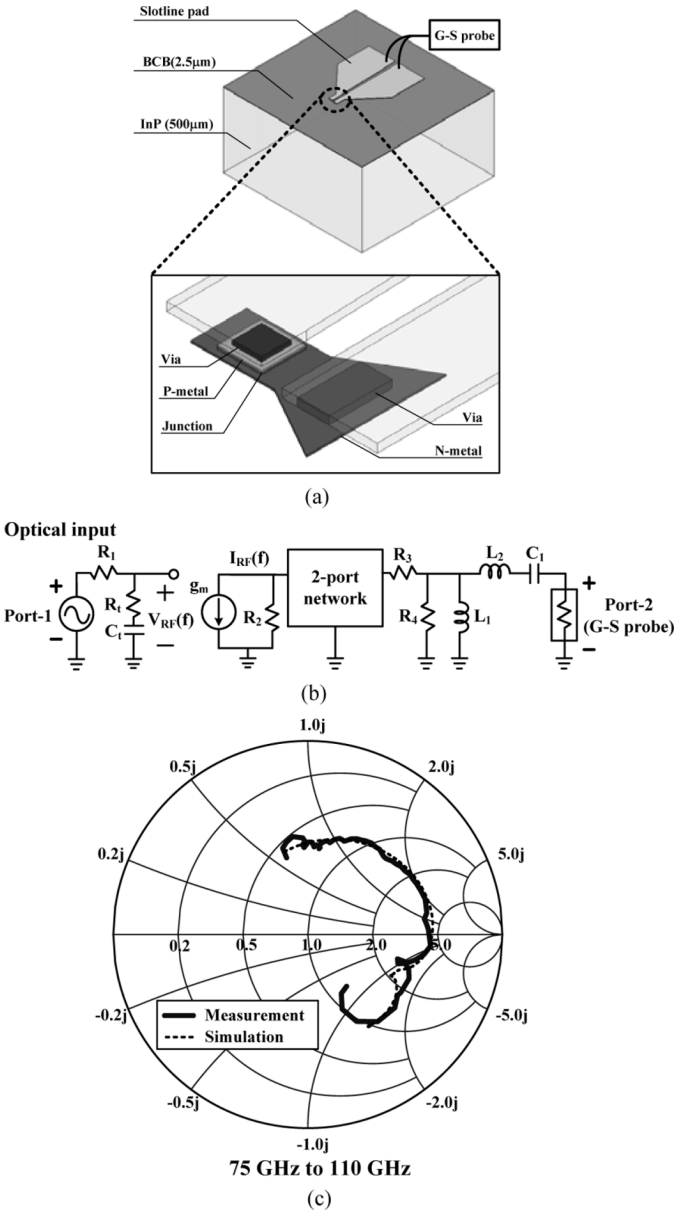

Fig. 2. (a) Configuration of the NBUTC-PD structure. (b) Corresponding two-port microwave network representation. (c) Measured and simulated input impedance of the structure.

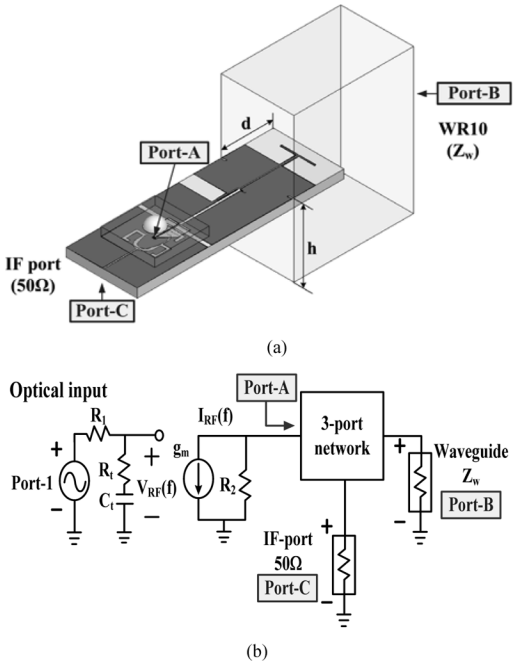

Fig. 3. (a) Configuration of the proposed photonic transmitter. (b) Corresponding three-port network representation.

of the PD is on an unground 900-μm-thick InP substrate for minimizing the impact of the metallic plate on the measured PD input impedance. Note that the InP substrate is finally ground to 100 μm in thickness for system integration, as depicted in Fig. 1(a). On the other hand, the PD structure is simulated with the finite-element-based full-wave simulator HFSS, and the simulated input impedance is employed for the PD network development. Here, the aforementioned two-port microwave network representation of the PD is obtained via curve fitting the measured input impedance. Specifically, the PD network together with the lumped-circuit elements ($R_3 = 13.68\ \Omega$, $R_4 = 537.6\ \Omega$, $L_1 = 2.1$ nH, $L_2 = 2.5$ pH, and $C_1 = 62.6$ fF) at Port 2 is used for describing the electrical characteristics of the PD structure. On the other hand, for mimicking the photonic MMW source input to the front end, i.e., optical input, the lumped circuit (with $R_t = 100\ \Omega$, $C_t = 4$ fF, $R_1 = 50\ \Omega$, $R_2 = 3000\ \Omega$, and $g_m = 12.4$ ms) is connected to Port 1. Note that the simulated/measured input impedance is obtained when Port 1 is open circuited. Fig. 2(c) demonstrates the measured input impedance of the PD structure, as well as the simulated one. As a consequence, good agreement is observed over the entire W-band.

With the two-port PD representation, the entire system can be represented as a three-port network through cascading the PD network with the network corresponding to the passive front-end circuitry. The proposed transmitter configuration along with its corresponding three-port network system representation is presented in Fig. 3(a) and (b), respectively. In Fig. 3(b), the lumped circuit connected to Port-A (optical port) is the same as the one on the left of the two-port PD network. Port-B (waveguide port) terminated with the wave impedance of the fundamental waveguide mode is for the representation of the modulated signal output from the transmitting antenna. Finally, Port-C (IF port) terminated with a matched load is for the representation of the IF data input. Note that the aforementioned coupling between the flip-chip bond pads and front-end circuitry is included in this network representation. Thanks to this representation, the entire system can be characterized with the commercial circuit simulator ADS in an effective manner.

B. Front-End Design and Characterization

In this section, the design and characterization of the transmitter front-end is briefly described. The transmitting horn antenna together with its feed structure is presented in Section II-B.1. Section II-B.2 describes the W-band BPF for bandlimiting the modulated photonic MMW source. Finally, the W-band BSF for filtering out the reflected MMW source from the feed is outlined in Section II-B.3.

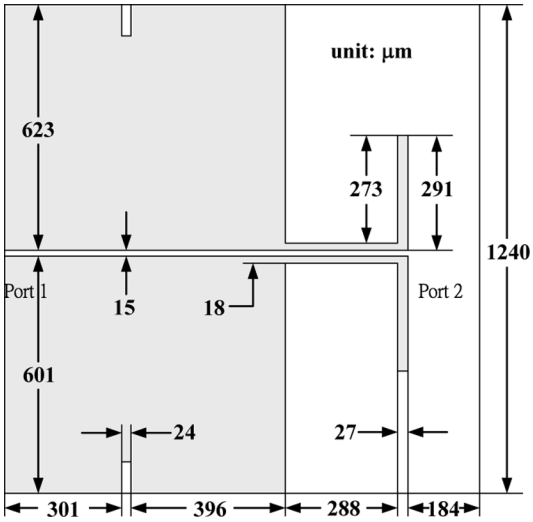

Fig. 4. Configuration and dimensions of the dipole-based waveguide feed structure.

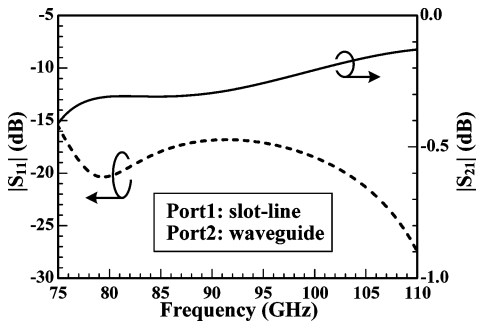

Fig. 5. Simulated S-parameter data of the feed structure with the WR-10 waveguide.

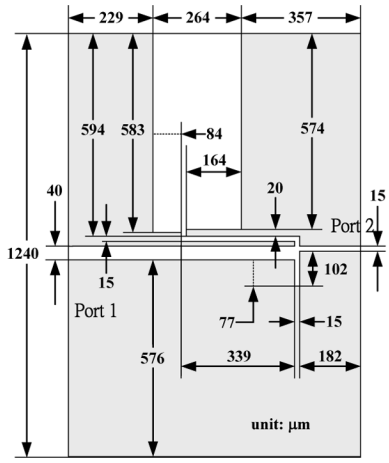

(a)

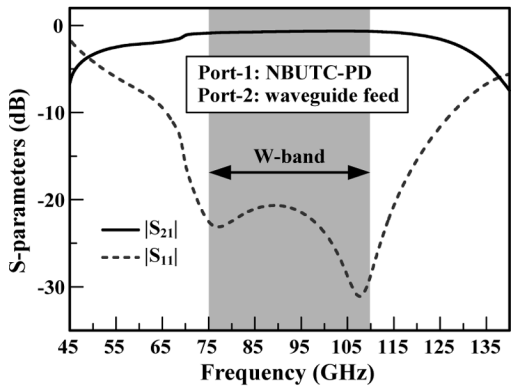

(b)

Fig. 6. (a) Configuration and dimensions of the W-band BPF. (b) Full-wave simulated result of the W-band BPF.

1) Transmitting Antenna and the Feed: The detailed configuration and dimensions of the dipole-based feed structure for the transmitting horn antenna are provided in Fig. 4. Note that all the dimensions are in micrometers and the region in light gray represents the metallic portion of the structure. In Fig. 4, the feed structure on a substrate of $\varepsilon_r = 8.6$ comprises a half-wavelength dipole fed by a slotline section. Similarly, the HFSS is employed for full-wave extraction of the S-parameter data of this waveguide feed and passive circuits of the front end described in Sections II-B.2 and II-B.3. As depicted in Fig. 3(a), the feed structure is placed in the waveguide opening with $d = 0.9$ mm and $h = 1.27$ mm for TE excitation. Specifically, the portion of the feed structure on the right of two alignment grooves on the ground is placed in the waveguide. With this feed configuration, the fundamental TE_{10} mode is effectively excited in the WR-10 waveguide with negligible insertion loss. Technically, the low insertion loss is achieved mainly owing to the ground plane in the vicinity of the dipole, which functions not only as a reflector for realization of the end-fire excitation, but as a structure for the suppression of the reflected wave. Fig. 5 shows the simulated S-parameter data of the feed with the WR-10 waveguide. Consequently, the insertion loss is less than 0.5 dB at the frequencies ranging from 75 to 110 GHz. Note that the waveguide and the feed structure are assumed lossless in the simulation.

2) W-Band BPF: The detailed configuration and dimensions of the W-band BPF realized with simple slotline short- and open-stub structures are provided in Fig. 6(a). Here, a stepped-impedance resonator design [27] is employed for the slotline open stub, which introduces a transmission pole at the center frequency of the W-band. On the other hand, the slotline short stub is employed for impedance tuning. Technically, the BPF fractional bandwidth is mainly related to the characteristic impedance of the short stub. Fig. 6(b) shows the full-wave simulated result of the W-band BPF. As a result, the BPF has a broad bandwidth poised for the W-band application.W-band

3) W-Band BSF: The configuration and dimensions of the W-band BSF realized with simple slotline short-subs are presented in Fig. 7(a) and (b). Fig. 7(b) provides the detailed dimensions of the portion outlined with a rectangular dashed box in Fig. 7(a). Similarly, the two transmission zeros at 81 and 100 GHz are introduced by the incorporation of the two bent slotline short-stub pairs A and B, respectively. Indeed, the transmission zeros can be separately adjusted via the electrical length of pairs A and B, respectively. The stopband rejection is also mainly related to the tapered slotline structure in between these two short-stub pairs. Note that the W-band BSF is located below the NBUTC-PD module, as depicted in Fig. 1(a). Hence, the PD layered structure, as well as the bond pillars and pads on top of the W-band BSF, is included in the analysis. Fig. 8 shows the

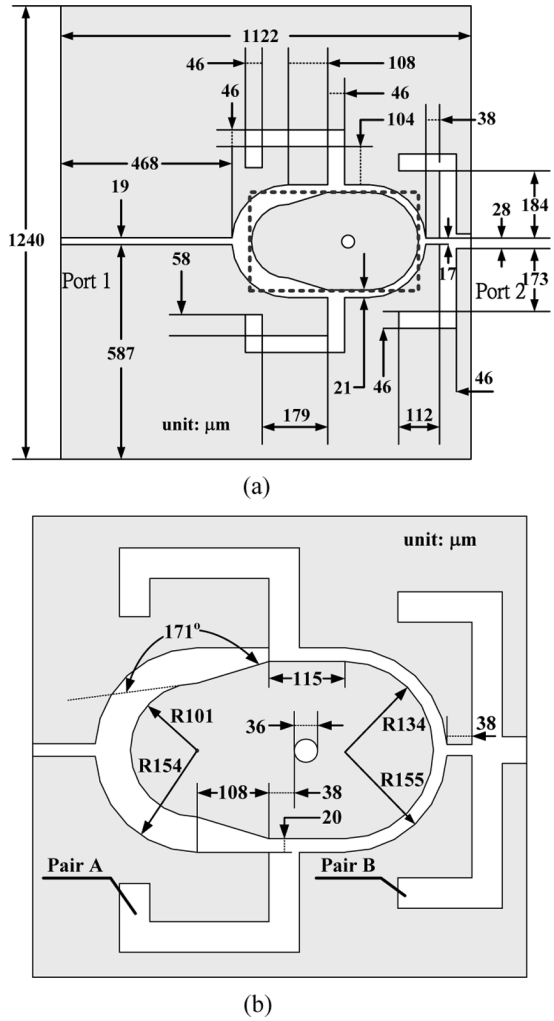

Fig. 7. (a) Configuration and dimensions of the W-band BSF. (b) Configuration and dimensions of the section outlined with a rectangular dashed box in Fig. 7(a).

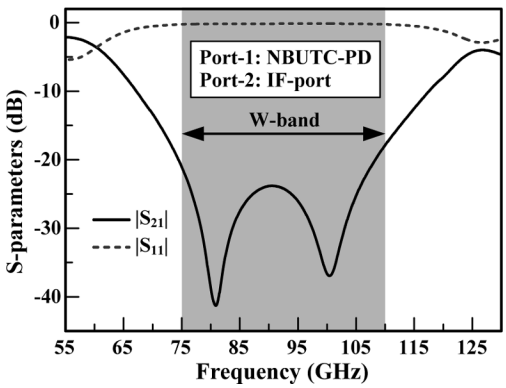

Fig. 8. Full-wave simulated results of the W-band BSF.

full-wave simulated S-parameter data of the W-band BSF. It is shown that the BSF has a high W-band rejection for alleviating IF signal leakage to the waveguide feed.

C. System Characterization

Section II-B outlines the NBUTC-PD modeling and describes the design and characterization of the front-end passive

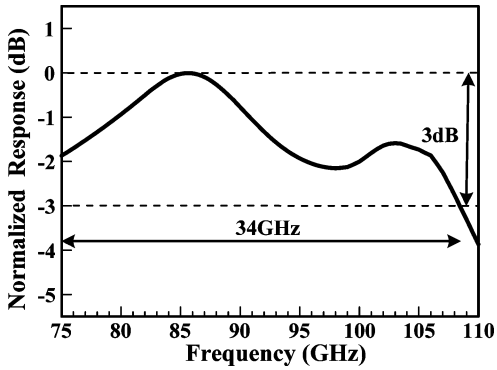

Fig. 9. Simulated O-E response of the demonstrated photonic transmitter.

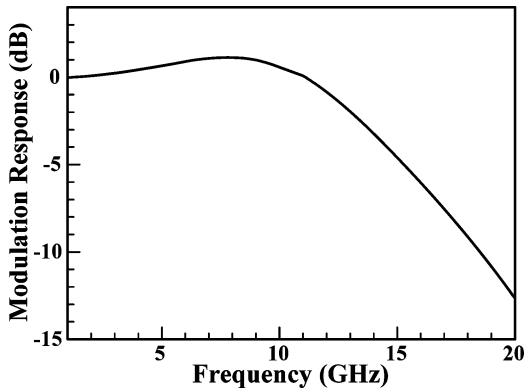

Fig. 10. Simulated IF modulation response of the demonstrated photonic transmitter.

circuits, respectively. Here, the characterization of the entire system is presented. Again, as presented in Fig. 3(b), the entire system, which comprises the NBUTD-module, waveguide feed, W-band BPF, and W-band BSF in a cascaded circuit topology, is represented as the three-port network. The three-port network can be characterized with the circuit solver ADS. Fig. 9 shows the simulated normalized O-E response of the transmitter, i.e., the insertion loss between optical port and the waveguide port. It is shown that the variation of the normalized O-E response is within 3 dB at the frequencies ranging from 75 to about 110 GHz. The simulated IF modulation response of the transmitter normalized to the one at dc is also presented in Fig. 10. It is shown that the 3-dB IF (video) bandwidth is as high as 13 GHz, which is crucial to the realization of a high-speed data transmission.

III. Experimental Setup and Verification

For design verification, the above-mentioned photonic transmitter is fabricated. Specifically, the dipole-based feed structure, RF choke, IF signal input port, and bond pillars and pads for flip-chip bonding are fabricated on a 150-μm-thick aluminium–nitride (AlN) substrate for good thermal conductivity (170 W/mK). The NBUTC-PD is integrated with the front-end circuitry through a flip-chip bonding process. Fig. 11(a) and (b) shows the top-view of the fabricated photonic transmitter without/with the integration of the NBUTC-PD, respectively. For system characterization, the experiments for measuring the

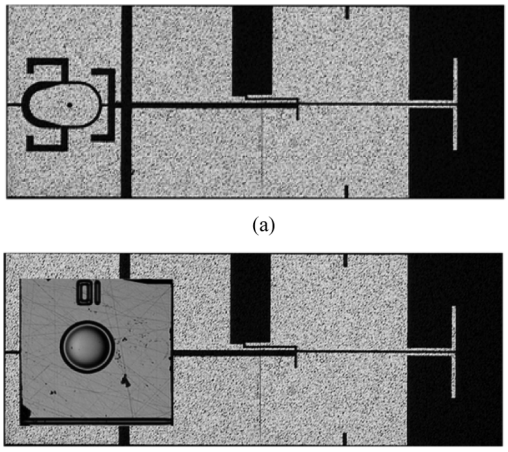

(a)

(b)

Fig. 11. Top view of the fabricated W-band photonic transmitter: (a) without the integration of the NBUTC-PD and (b) with the integration of the NBUTC-PD.

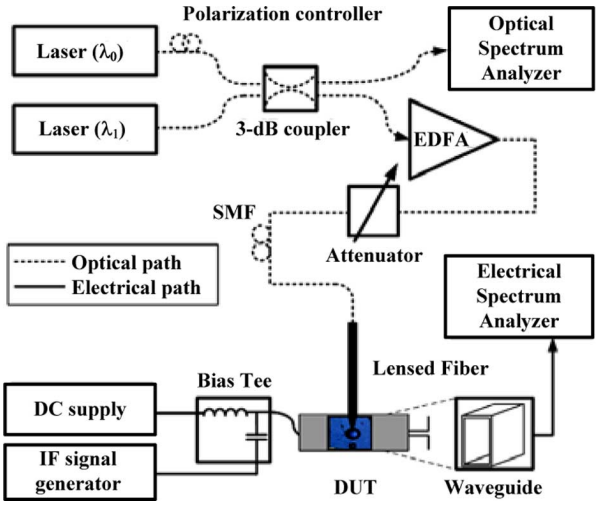

Fig. 12. Experimental setup for the O-E response measurement.

normalized O-E response, video bandwidth, and the bit-error rate (BER) of a high-speed wireless link are performed. Fig. 12 outlines the experimental setup for the O-E response measurement. In the measurement, the photonic MMW source, i.e., LO source of the transmitter, is generated by the heterodyne-beating technique with the center laser wavelength (λ_0) at around 1550 nm. Specifically, the LO source at different wavelengths is generated by changing the laser wavelength (λ_1). The generated photonic MMW source amplified with the erbium-doped fiber amplifier (EDFA) passes through a tunable optical attenuator. Finally, the photonic MMW source focused with the microlens illuminates the backside of the diced NBUTC-PD, which is biased at -3 V with a 4-mA photocurrent. Meanwhile, the IF signal, i.e., the input signal, pumped into the NBUTC-PD through a bias-tee and a microwave probe is up-converted with the LO source. The up-converted input signal propagates through a WR-10 waveguide connected to an electrical spectrum analyzer. Fig. 13 shows the measured normalized O-E response of the demonstrated photonic transmitter compared

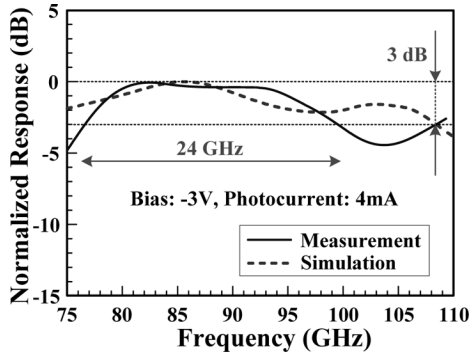

Fig. 13. Measured and simulated O-E response.

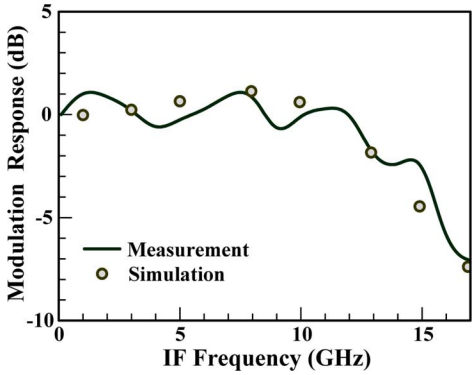

Fig. 14. Measured and simulated IF modulation response.

to the simulated one. Again, this O-E response is measured by changing the laser wavelength (λ_1) to generate a MMW source at different frequencies. As a consequence, the measurement data are in reasonably good agreement with the simulation data over a broad bandwidth (77–100 GHz). The discrepancy at the higher frequencies is likely owing to the parasitics attributed to the probe feed. The measured normalized 3-dB O-E bandwidth is around 24 GHz ranging from 76 to 100 GHz. Similarly, the normalized IF modulation response of the transmitter is measured by changing the IF signal frequency. Fig. 14 demonstrates the measured normalized response of the transmitter compared to the simulated one. It is shown that the measured response is in very good agreement with the simulated from dc to 17 GHz, and the variation of the video bandwidth, ranging from the dc to about 13 GHz, is within 3 dB.

Next, the experimental setup for the high-speed wireless link is outlined in Fig. 15. In the setup, the 20-Gb/s pseudo-random binary sequence (PRBS) input data is fed into the IF port directly to modulate the bias point of the NBUTC-PD. The sinusoidal LO source (93 GHz) illuminates the backside of NBUTC-PD. The up-converted input data is then delivered to the WR-10 waveguide connected to the horn antenna for data transmission. A MMW receiver is employed for envelope detection of the received signal. The receiver front-end comprises a W-band horn antenna, a W-band low-noise-amplifier (LNA) (Militech: LNA-10–02150), and a fast W-band power detector (Militech: DXP-10-RPFW0). The down-converted data signal from the receiver front-end is then amplified, recorded, and analyzed by an

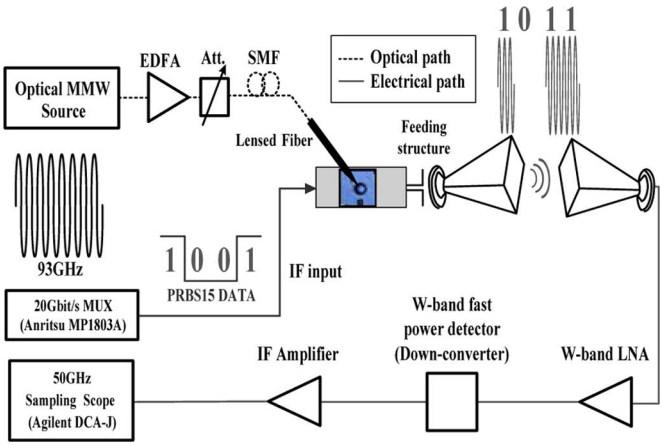

Fig. 15. Experimental setup for the high-speed wireless link.

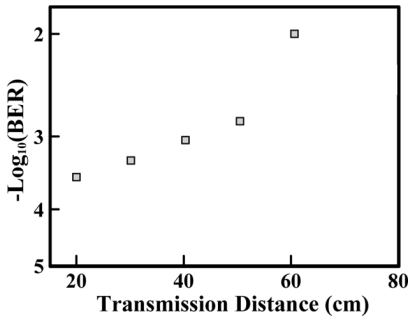

Fig. 16. $-\log_{10}(\mathrm{BER})$ versus transmission distance for the 20-Gb/s wireless link.

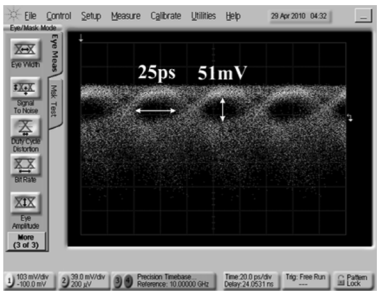

Fig. 17. Measured 20-Gb/s eye pattern at 20 cm.

IF amplifier, high-speed sampling scope, and an error detector, respectively. Fig. 16 shows $-\log_{10}(\mathrm{BER})$ versus transmission distance for 20 Gb/s (PRBS: $2^{15}-1$) on–off keying (OOK) data transmission. As a result, with 9-mA operation current, 20 Gb/s (BER less than 1×10^{-3}) transmission distance is around 60 cm. Also, with 9-mA photocurrent, the corresponding 20-Gb/s eye pattern at 20 cm is given in Fig. 17. It is shown that clear eye openings for 20 Gb/s is observed with long word-length ($2^{15}-1$). Compared to our previously demonstrated photonic transmitter [28], the data rate is significantly increased.

For demonstration of the effectiveness of the proposed transmitter design, the data rate and BER of the proposed design, our previous design, and other reported designs [1], [18], [29]–[31] are listed in Table I. In Table I, with the OOK modualtion, it is shown that the demonstrated transmitter has a relatively high data rate with a reasonable BER.

TABLE I
COMPARISON OF THE PERFORMANCE OF THE PROPOSED TRANSMITTER TO THE REPORTED DESIGNS

Transmitter Designs	Operating Band/Frequency	Data Rate (modulation)	BER
This work	W band	20 Gb/s(OOK)	8e-4
Previous work [21]	W band	12.5 Gb/s(OOK)	1e-12
[1]	120 GHz	10 Gb/s (OOK)	1e-12
[18]	120 GHz	10 Gb/s (OOK)	1e-9
[29]	V band	12.5 Gb/s (OOK)	1e-8
[30]	250GHz	8 Gb/s (OOK)	1e-8
[31]	V band	27Gb/s(16-QAM OFDM)	4.2e-3

IV. Conclusion and Future Work

A high-speed W-band integrated photonic transmitter with a broad IF modulation bandwidth, as well as a wide O-E bandwidth, has been presented. The demonstrated integrated photonic transmitter for high-data-rate wireless transmission comprises the NBUTC-PD and the broadband front-end circuitry. Technically, the BPF is employed to further increase the isolation between the IF signal input and LO source output. The enhanced isolation is shown to be the key to the broad system video bandwidth. The effectiveness of the proposed transmitter design is experimentally verified. On the other hand, a high data-rate (20 Gb/s) RoF communication using the demonstrated photonic transmitter has been presented. Future work will focus on further improvement on the transmission distance, BER, as well as the data rate. The increase of channel capacity of the RoF communication system through incorporating an adaptive antenna array into the proposed transmitter will also be investigated.

Acknowledgment

The authors wish to thank Prof. C.-L. Pan, Department of Physics, National Tsing-Hua University, Hsinchu, Taiwan, Prof. C.-T. Lin, Prof. J. Chen, and Dr. W.-J. Jiang, all with the Institute of Photonic, National Chiao-Tung University, Hsinchu, Taiwan, and Prof. S. Chi, Department of Electrical Engineering, Yuan-Ze University, Jhongli, Taiwan, for their technical support on the system measurement.

References

[1] A. Hirata, H. Takahashi, R. Yamaguchi, T. Kosugi, K. Murata, T. Nagatsuma, N. Kukutsu, and Y. Kado, "Transmission characteristics of 120-GHz-band wireless link using radio-on-fiber technologies," *IEEE J. Lightw. Technol.*, vol. 26, no. 8, pp. 2338–2344, Aug. 2008.

[2] M. Beltrán and R. Llorente, "60-GHz ultra-wideband radio-over-fiber system using a novel photonic monocycle generation," *IEEE Trans. Microw. Theory Tech.*, vol. 58, no. 6, pp. 1609–1620, Jun. 2010.

[3] Y. L. Guennec and R. Gary, "Optical frequency conversion for millimeter-wave ultra-wideband-over-fiber systems," *IEEE Photon. Technol. Lett.*, vol. 19, no. 7, pp. 996–998, Jul. 2007.

[4] S. Fu, W. Zhong, Y. J. Wen, and P. Shum, "Photonic monocycle pulse frequency up-conversion for ultrawideband-over-fiber applications," *IEEE Photon. Technol. Lett.*, vol. 20, no. 6, pp. 1006–1008, Jun. 2008.

[5] J. Yu, G.-K. Chang, Z. Jia, A. Chowdhury, M.-F. Huang, H.-C. Chien, Y.-T. Hsueh, W. Jian, C. Liu, and Z. Dong, "Cost-effective optical millimeter technologies and field demonstrations for very high throughput wireless over fiber access systems," *IEEE J. Lightw. Technol.*, vol. 28, no. 8, pp. 2376–2397, Aug. 2010.

[6] M. F. Huang, J. Yu, Z. Jia, and G. K. Chang, "Simultaneous generation of centralized lightwaves and double/single sideband optical millimeter wave requiring only low-frequency local oscillator signals for radio-over-fiber systems," *J. Lightw. Technol.*, vol. 26, no. 8, pp. 2653–2662, Aug. 2008.

[7] L. Chen, H. Wen, and S. Wen, "A radio-over-fiber system with a novel scheme for millimeter-wave generation and wavelength reuse for up-link connection," *IEEE Photon. Technol. Lett.*, vol. 18, no. 10, pp. 2056–2058, Oct. 2006.

[8] X. Zhang, B. Liu, J. Yao, K. Wu, and R. Kashyap, "A novel millimeterwave-band radio-over-fiber system with dense wavelength-division multiplexing bus architecture," *IEEE Trans. Microw. Theory Tech.*, vol. 54, no. 2, pp. 929–937, Feb. 2006.

[9] J. H. Seo, C. S. Choi, Y. S. Kang, Y. D. Chung, J. Kim, and W. Y. Choi, "SOA-EAM frequency up/down-converters for 60-GHz bi-directional radio-on-fiber systems," *IEEE Trans. Microw. Theory Tech.*, vol. 54, no. 2, pp. 959–966, Feb. 2006.

[10] H. Ito, S. Kodama, Y. Muramoto, T. Furuta, T. Nagatsuma, and T. Ishibashi, "High-speed and high-output InP–InGaAs uni-traveling-carrier photodiodes," *IEEE J. Sel. Topics Quantum Electron.*, vol. 10, no. 7/8, pp. 709–727, Jul./Aug. 2004.

[11] Y.-S. Wu and J.-W. Shi, "Dynamic analysis of high-power and high-speed near-ballistic uni-traveling carrier photodiodes at W-band," *IEEE Photon. Technol. Lett.*, vol. 20, no. 7, pp. 1160–1162, Jul. 2008.

[12] J. W. Shi, F.-M. Kuo, C.-J. Wu, C. L. Chang, C. Y. Liu, C.-Y. Chen, and J. I. Chyi, "Extremely high saturation current-bandwidth product performance of a near-ballistic uni-traveling-carrier photodiode with a flip-chip bonding structure," *IEEE J. Quantum Electron.*, vol. 46, no. 1, pp. 80–86, Jan. 2010.

[13] K. Kato, "Ultrawide-band/high-frequency photodetectors," *IEEE Trans. Microw. Theory Tech.*, vol. 47, no. 7, pp. 1265–1281, Jul. 1999.

[14] J.-W. Shi, Y.-S. Wu, C.-Y. Wu, P.-H. Chiu, and C.-C. Hong, "High-speed, high-responsivity, and high-power performance of near-ballistic uni-traveling-carrier photodiode at 1.55-μm wavelength," *IEEE Photon. Technol. Lett.*, vol. 17, no. 9, pp. 1929–1931, Sep. 2005.

[15] A. Hirata, H. Ishii, and T. Nagatsuma, "Design and characterization of a 120-GHz millimeter-wave antenna for integrated photonic transmitters," *IEEE Trans. Microw. Theory Tech.*, vol. 49, no. 11, pp. 2157–2162, Nov. 2001.

[16] J.-W. Shi, F.-M. Kuo, Y.-S. Wu, N.-W. Chen, P.-T. Shih, C.-T. Lin, W.-J. Jiang, E.-Z. Wong, J. Chen, and S. Chi, "W-band photonic transmitter-mixer based on high-power near-ballistic uni-traveling-carrier photodiodes for BPSK and QPSK data transmission under bias modulation," *IEEE Photon. Technol. Lett.*, vol. 21, no. 8, pp. 1039–1041, Aug. 2009.

[17] N. Shimizu and T. Nagatsuma, "Sub-terahertz radiation from a photodiode-integrated patch antenna array," in *Int. Microw. Photon. Top. Meeting*, 2005, pp. 339–342.

[18] A. Hirata, T. Kosugi, N. Meisl, T. Shibata, and T. Nagatsuma, "High-directivity photonic emitter using photodiode module integrated with HEMT amplifier for 10-Gbit/s wireless link," *IEEE Trans. Microw. Theory Tech.*, vol. 52, no. 8, pp. 1843–1850, Aug. 2004.

[19] P. Otero, G. V. Eleftheriades, and J. R. Mosig, "Integrated modified rectangular loop slot antenna on substrate lenses for millimeter- and submillimeter-wave frequencies mixer applications," *IEEE Trans. Antennas Propag.*, vol. 46, no. 10, pp. 1489–1497, Oct. 1998.

[20] Y. Qian, W. R. Deal, N. Kaneda, and T. Itoh, "A uni-planar quasi-Yagi antenna with wide bandwidth and low mutual coupling characteristics," in *IEEE Antennas Propag. Symp. Dig.*, Jul. 1999, vol. 2, pp. 924–927.

[21] Y.-S. Wu, N.-W. Chen, and J.-W. Shi, "A W-band photonic transmitter/mixer based on high-power near-ballistic uni-traveling-carrier photodiode (NBUTC-PD)," *IEEE Photon. Technol. Lett.*, vol. 20, no. 11, pp. 1799–1801, Nov. 2008.

[22] N. Kaneda, W. R. Deal, Y. Qian, R. Waterhouse, and T. Itoh, "A broadband planar quasi-Yagi antenna," *IEEE Trans. Antennas Propag.*, vol. 50, no. 8, pp. 1158–1160, Aug. 2002.

[23] N. Kaneda, Y. Qian, and T. Itoh, "A broadband CPW-to-waveguide transition using quasi-Yagi antenna," in *IEEE MTT-S Int. Microw. Symp. Dig.*, Boston, MA, Jun. 2000, vol. 2, pp. 617–620.

[24] T.-H. Lin and R.-B. Wu, "CPW to waveguide transition with tapered slotline probe," *IEEE Microw. Wireless Compon. Lett.*, vol. 11, no. 10, pp. 314–316, Jul. 2001.

[25] V. S. Möttönen, "Wideband coplanar waveguide-to-rectangular waveguide transition using fin-line taper," *IEEE Microw. Wireless Compon. Lett.*, vol. 15, no. 2, pp. 119–121, Feb. 2005.

[26] V. S. Möttönen and A. V. Räisänen, "Novel wideband coplanar waveguide-to-rectangular waveguide transition," *IEEE Trans. Microw. Theory Tech.*, vol. 52, no. 8, pp. 1836–1842, Aug. 2004.

[27] D. M. Pozar, *Microwave Engineering*, 3rd ed. New York: Wiley, 2004.

[28] H.-J. Tsai, N.-W. Chen, F.-M. Kuo, and J.-W. Shi, "Front-end design of W-band integrated photonic transmitter with wide optical-to-electrical bandwidth for wireless-over-fiber application," in *IEEE MTT-S Int. Microw. Symp. Dig.*, Anaheim, CA, May 23–28, 2010, pp. 740–743.

[29] M. Weiss, M. Huchard, A. Stohr, B. Charbonnier, S. Fedderwitz, and D. S. Jager, "60-GHz photonic millimeter-wave link for short- to medium-range wireless transmission up to 12.5 Gb/s," *J. Lightw. Technol.*, vol. 26, no. 8, pp. 2424–2429, Aug. 2008.

[30] H.-J. Song, K. Ajito, A. Hirata, A. Wakatsuki, Y. Muramoto, T. Furuta, N. Kukutsu, T. Nagatsuma, and Y. Kado, "8 Gbit/s wireless data transmission at 250 GHz," *Electron. Lett.*, vol. 45, pp. 1121–1122, Oct. 2009.

[31] M. Weiss, A. Stohr, B. Charbonnier, and S. Fedderwitz, "27 Gbit/s photonic wireless 60 GHz transmission system using 16-QAM OFDM," in *Int. Microw. Photon. Top. Meeting*, Valencia, Spain, Oct. 14–16, 2009, pp. 1–3.

Nan-Wei Chen (M'03) received the B.S. degree in atmospheric sciences and M.S. degree in space sciences from National Central University, Jhongli, Taiwan, in 1993 and 1995, respectively, and the Ph.D. degree in electrical engineering from the University of Illinois at Urbana-Champaign, in 2004.

From 1998 to 2004, he was a Research Assistant with the Center for Computational Electromagnetics, University of Illinois at Urbana-Champaign, where he was involved with time-domain integral equation methods for the solution of scattering and radiation problems. From 2004 to 2009, he was an Assistant Professor of electrical engineering with the National Central University. Since 2010, he has been an Associate Professor of communications engineering with Yuan Ze University, Jhongli, Taiwan. His research interests include computational electromagnetics with a special emphasis on time-domain integral equations, periodic structures, and MMW antennas and passive circuits.

Prof. Chen was the recipient of the Raj Mittra Outstanding Research Award of the University of Illinois at Urbana-Champaign in 2004 and the Best Article Award of the Chinese Geoscience Union in 2010.

Hsuan-Ju Tsai was born in Taoyuan, Taiwan, on November 19, 1984. He received the B.S. degree in mechatronic technology from National Taiwan Normal University, Taipei, Taiwan, in 2008, and the M.S.E.E. degree in electrical engineering from National Central University, Taoyuan, Taiwan, in 2010.

His research interests include the design and analysis of microwave/MMW circuits and ultra-high-speed photonics and their applications to communication.

Fon-Ming Kuo was born in Kaohsiung, Taiwan, on February 12, 1986. He received the B.S. degree in electrical engineering from National Central University, Jhongli, Taiwan, and is currently working toward the M.S. degree in electrical engineering at National Central Unversity.

His research is mainly focus on MMW high-power PDs and their applications. He is also involved in RF/microwave semiconductor opto-electronic devices for communication, such as vertical-cavity surface-emitting lasers (VCSELs), avalanche photodiodes (APDs), and high-speed light-emitting diodes (LEDs).

Jin-Wei Shi (S'02–M'02) was born in Kaohsiung, Taiwan, on January 22, 1976. He received the B.S. degree in electrical engineering from National Taiwan University, Taipei, Taiwan, in 1998, and the Ph.D. degree from the Graduate Institute of Electro-Optical Engineering, National Taiwan University, in 2002.

From 2000 to 2001, he was a Visiting Scholar with the University of California at Santa Barbara. From 2002 to 2003, he ws a Post-Doc Researcher with the Electronic Research and Service Organization (ERSO), Industrial Technology Research Institute (ITRI). In 2003, he joined the Department of Electrical Engineering, National Central University, Taoyuan, Taiwan, where he is currently an Associate Professor. He has authored or coauthored over 70 journal papers and 100 conference papers. He holds 13 patents. His current research interests include ultrahigh-speed/power opto-electronic devices such as photodetectors, electro-absorption modulators, sub-millimeter wave photonic transmitters, and semiconductor lasers.

Prof. Shi was the invited speaker of the 2002 IEEE LEOS, 2005 SPIE Optics East, 2007 AMWP, and 2008 AOE. He was a member of the Technical Program Committee of OFC from 2009 to 2011. He was the recipient of the 2007 Excellence Young Researcher Award of the Association of Chinese IEEE.